Palladosilicide, Pd_2Si, a new mineral from the Kapalagulu Intrusion, Western Tanzania and the Bushveld Complex, South Africa

L. J. CABRI[1]*, A. M. MCDONALD[2], C. J. STANLEY[3], N. S. RUDASHEVSKY[4], G. POIRIER[5], H.R. WILHELMIJ[6], W. ZHE[7], AND V.N. RUDASHEVSKY[4]

[1]Cabri Consulting Inc., 700-702 Bank Street, PO Box 14087, Ottawa, Ontario, Canada K1S 3V0
[2]Department of Earth Sciences, Laurentian University, Ramsey Lake Road, Sudbury, Ontario, Canada P3E 2C6
[3]Natural History Museum, Cromwell Road, London SW7 5BD, UK
[4] CNT Instruments LTD, Svetlanovsky Ave. 75-41, St. Petersburg, Russia
[5]Canadian Museum of Nature, Earth Science Research Services, 1740 Pink Road, Gatineau, Quebec J9J 3N7 (formerly Canmet, Ottawa)
[6] Ore Deposit Geologist, 3 Norham End, North Oxford OX2 6SG, England (formerly Lonmin-Goldstream JV, Australia)
[7] Central Analytical Facility, Laurentian University, Ramsey Lake Road, Sudbury, Ontario, Canada P3E 2C6

Abstract

Palladosilicide, Pd_2Si, is a new mineral (IMA 2104-080) discovered in chromite-rich samples from the Kapalagulu intrusion, western Tanzania (30°03'51"E 5°53'16"S and 30°05'37"E 5°54'26"S) and from the UG-2 chromitite, Bushveld complex, South Africa. A total of 13 grains of palladosilicide, ranging in size from 0.7 to 39.1 μm (ECD), were found. Synthetic Pd_2Si is hexagonal, space group *P*-62*m*, with *a* = 6.496(5), *c* = 3.433(4) Å, *V* = 125.5(1) $Å^3$, *c*:*a* = 0.529 with Z = 3. Strongest lines calculated from the powder pattern (Anderko and Schubert 1953) are [*d* in Å (*I*) (*hkl*)] 2.3658 100 111; 2.1263 37 120; 2.1808 34 021; 3.240 20 110; 1.8752 19 030; 1.7265 12 002; 1.3403 11 122; 1.2089 10 231. The calculated density for three analyses varies from 9.562 to 9.753 g cm^{-3}. Palladosilicide is considered to be equivalent to synthetic Pd_2Si based on results from electron back-scattered diffraction (EBSD) analyses. Reflectance data in air for the four COM wavelengths are [λ nm, R_1 (%) R_2 (%)] 470 49.6 52.7; 546 51.2 53.8; 589 51.6 53.7; 650 51.7 53.3 and the mineral is bright creamy white against chromite, weakly bireflectant, and does not display discernable pleochroism or twinning. It is weakly anisotropic, has weak extinction and rotation tints in shades of blue and olive green. Electron probe microanalyses of palladosilicide yields a simplified formula of Pd_2Si, slightly metal-rich (from 2.058 to 2.123).

Introduction

Palladosilicide (Pd_2Si) is a new mineral recently discovered in two different localities. One was the Platinum-Group Element (PGE)-chromite horizon of the Kapalagulu Intrusion near the eastern shore of Lake Tanganyika, western Tanzania, with the mineral being discovered in diamond drill cores KPD 044 (30°03'51"E 5°53'16"S; sample D396) and KPD 024 (30°05'37"E 5°54'26"S; sample 10369), and the second from the UG-2 chromitite, Bushveld Complex, RSA. In both cases the mineral was discovered in heavy mineral concentrates collected for detailed

quantitative mineralogical investigations associated with mineral processing and optimization; details regarding these concentrates were reported in Cabri (2004) for the Tanzanian samples and from a flotation tailing for the UG-2 chromitite Cabri et al. (2008).

Disseminated copper and nickel sulphide in harzburgite near the base of the Kapalagulu Intrusion has been known for over a century. The Kapalagulu Intrusion lies near the eastern shore of Lake Tanganyika in Western Tanzania and forms part of a series of mafic intrusions that include Musongati and Kabanga, known as the Burundi Nickel Belt (Figure 1). In the late 1990's, Broken Hill Proprietary found Pt-Pd mineralization associated with Ni-bearing lateritic regolith. During 2002 and 2003, Goldstream Mining, in partnership with Lonmin plc, identified sulphide-chromitite horizons in harzburgite below the lateritic regolith that contain PGE with grades of between 1 and 12 g/t PGE (Wilhelmij and Joseph 2004). The PGE mineralization occurs in the Lower Ultramafic Sequence of the Kapalagulu Intrusion that is preserved in a dyke-like extension to the Upper Mafic Sequence, known as the Lubalisi zone (Figure 2).

The upper Critical Zone of the Bushveld Complex hosts the largest concentration of PGEs in the world (Schouwstra et al. 2008). The UG-2 Reef is a PGE-bearing chromitite layer, usually 1 m thick but can vary from ~ 0.4 to up to 2.5 m, developed some 20 to 400 metres below the better known Merensky Reef (Schouwstra et al. 2008). A comprehensive review of the UG-2 may be found in Cawthorn (2002).

Mineral Name and type material

The mineral is named after the two essential chemical components, palladium and silicon. The mineral and name were approved by the IMA – Commission on New Minerals, Nomenclature and Classification (CNMNC) on 3 December, 2014. Part of the holotype has been deposited

in the collections of the Canadian Museum of Nature, Gatineau, Quebec, Canada, catalogue number CMNMC 86891.

Occurrence and associated minerals

In both occurrences palladosilicide was found in monolayer polished sections of high-grade gravity concentrates made with an earlier model manual hydroseparator (HS-02) by one of us (NSR); see for example, Rudashevsky et al. (2004), and McDonald et al. (2014) who report a large number of PGM from the Coldwell complex (Ontario) found by using the computer-operated newer model hydroseparator (HS-11).

A total of 13 grains of palladosilicide were found, ranging in size from 0.7 to 39.1 µm (ECD). Four of the twelve palladosilicide grains found in the Tanzanian samples were imaged (Figure 3). They came from two unoxidized samples, both 30-cm long: DDH KPD044 (D-396, at a depth of between 169.9 and 170.2m) and from DDH KPD024 (010369, at a depth of between 53.0 and 53.3m). The mineralogical study of pristine sulphide-bearing samples as well as oxidized samples from the regolith forms part of a separate publication (Wilhelmij and Cabri, in prep.).

Common heavy minerals in the samples include chromite, pentlandite, pyrrhotite/troilite; minor minerals were chalcopyrite and magnetite; and rare to trace minerals include gudmundite, arsenopyrite, zircon, galena, and anglesite. Six the palladosilicide grains were free, but others were attached to chromite (n=5) or locked in chromite (n=2). The total frequency of precious metal minerals found in the three samples ranged from 93 for sample D396 to 137 for sample 10369, which included some found during image analysis of unconcentrated sample splits. Table 1 illustrates a typical range of precious metal minerals found in heavy mineral concentrates with their relative abundances for sample 10369.

The concentrates of the UG-2 tailing sample are dominated by chromite with a few PGM consisting of free laurite (ideally RuS_2) particles, a graphic intergrowth of tetraferroplatinum (ideally PtFe) in pyrrhotite, isoferroplatinum (ideally Pt_3Fe) included in pentlandite, sobolevskite (ideally $PdBi_2$) attached to a larger particle of orthopyroxene, and a smaller (3.8 µm ECD) inclusion of kotulskite (ideally PdTe) included in an undefined Cu-Ag telluride (22.2 µm ECD), which is itself attached to a larger particle of chromite. A single free particle of the new Pd_2Si mineral 39.1 µm in size (ECD) with an unidentified Pd-Sn mineral (taimyrite?) 6.3 µm in size (ECD) and undetermined very small (~1 to 3 µm in maximum width) bright metallic inclusions was found after making additional concentrations.

Physical and optical properties

Palladosilicide appears bright creamy white against the surrounding plastic, grains of chromite, and its inclusions of a Pd-(Cu)-Sn mineral (taimyrite?), unknown1 (gray) and unknown2 (bright white), as shown in Figure 4. The area of the Pd-(Cu)-Sn mineral is larger after repolishing and the two unknown inclusions now appear, not visible on the earlier SEM BSE image. Palladosilicide has an anhedral to subhedral habit, a metallic luster, is weakly bireflectant and does not display discernible reflection pleochroism or twinning. It is weakly anisotropic, has a weak extinction and rotation tints in shades of light blue and olive green. Micro-indentation hardness could not be measured due to small grain size. Tenacity and streak were not determined, and cleavage, partings, and fracture were not observed.

The reflectance spectrum was measured on the grain from the UG-2 in air and oil and is given in Figure 5; the colour values are listed in Table 2 and reflectance data in Table 3 and no internal reflections were noted.

Chemical composition

Chemical analyses using energy dispersion spectrometry (EDS) and a Camscan Microspec-4DV scanning electron microscope with a Link AN-10000 detector. The operating conditions included an accelerating beam voltage of 30 kV, a beam current of 1-2 nA, a beam diameter of 1 μm and counting times of 50-100 s. Standards used were Si, diopside $CaMgSi_2O_6$; As, InAs; other elements, pure metals.

The analyses of three grains from the Kapalagulu intrusion gave close to stoichiometric compositions (based on 3 atoms): $(Pd_{1.75}Ni_{0.20}Cu_{0.08}Fe_{0.03}Sn_{0.03}Pt_{0.02})_{2.11}(Si_{0.72}As_{0.16})_{0.88}$ (shown in Figure 3); $(Pd_{1.53}Ni_{0.23}Pt_{0.07}Sn_{0.07}Cu_{0.05}Fe_{0.03})_{1.98}Si_{1.02}$ (shown in Figure 3); and $(Pd_{1.62}Ni_{0.23}Cu_{0.05}Pt_{0.07})_{2.01}(Si_{0.96}As_{0.03})_{0.99}$ (shown in Figure 2), as well as on one grain from the UG-2 sample $(Pd_{1.61}Ni_{0.22}Cu_{0.08}Sn_{0.05}Pt_{0.03})_{1.99}(Si_{0.90}As_{0.12})_{1.02}$ (shown in Figure 4). Although Ag, Se, Sb, Te, Au, Pb, and Bi were sought for in sample 10369 (grains 6 and 18), and sample D396 (grain 21), these elements were not detected. For the UG-2 grain, Sb was sought and not detected.

Electron microprobe analyses (WDS) were later carried out on two grains with a JEOL 8900L electron microprobe at CANMET-MMSL in Ottawa (Table 4). Operating conditions were, 20 kV accelerating current, 40 nA beam current, one μm spot size, raw data were corrected using a ZAF matrix correction. The following standards and analytical lines were used: Si *Kα*, Si metal; Cr *Kα*, chromite; Pd Lα, Pd metal; Ag *Lβ*, $Au_{60}Ag_{40}$; S *Kα*, pyrite; Se *Lα*, Se metal; Ni *Kα*, NiSb; Te *Lα*, Te metal; P *Kα*, apatite; Sb *Lα*, NiSb; As *Lα*, $FeAs_2$; Fe *Kα*, pyrite; Pt *Mα*, Pt metal; Sn *Lα*, Sn metal; Pb *Mα*, galena; Cu *Kα*, chalcopyrite; Rh *Lα*, Rh metal. Counting times were 20 s peak and 10 s backgrounds on both sides, except for Pd and Pb which were measured for 50 s peak and 25 s background on both sides. The results, calculated on the basis of 3 atoms, show a slight excess of Pd over Si (Table 5).

Crystallography

The small grain size and the presence of inclusions precluded analyzing palladosilicide by standard PXRD methods. The crystallographic properties of the mineral were thus studied by Electron Backscatter Diffraction (EBSD). Preliminary SEM-EDS analyses of the grain selected for EBSD analysis (Grain 6, 10369 45-1) confirm major Pd and Si, along with trace Ni, Pt, As and Sn. The grain studied was found to contain sub-millimeter inclusions, representing perhaps 5% of the total area, of an unidentified Ag-Te± Sn mineral.

EBSD analyses were carried out on grain 6 (10369 45-1) from Kapalagulu with a JEOL 6400 SEM equipped with a HKL EBSD system (HKL Technology Inc., Oxford Instruments Group), an accelerating voltage of 20 kV, a beam current of 2.4 nA and a sample-to-camera working distance of 130 mm. The system was calibrated using a crystal of synthetic Si. Care was also taken to avoid collected EBSD (Kikuchi) patterns from those areas proximal to the Ag-Te inclusion (Figure 6). Frames were collected for 20 ms, with 64 frames per image, both being selected so as to mitigate degradation of the epoxy surrounding the grain, this being found to be quite unstable under the electron beam. Channel5 software (Oxford Instruments; Day and Trimby, 2004) was used to collect Kikuchi (EBS) patterns along with pattern matching and interpretation (Figure 7). It is noteworthy that the Kikuchi patterns from three subareas were found to be near identical, indicating all three areas are nearly identical in crystallographic orientation and thus that the grain being studied is presumably close to being single.

From each of the Kikuchi patterns obtained (n = 3), seven strong bands were manually selected and used for matching purposes. Matching was accomplished through comparison with Kikuchi patterns calculated for synthetic Pd_2Si, along with those for a number of synthetic phases having similar stoichiometries, including (with the corresponding

International Crystal Structure Database, ICSD, number) Pd_2B (ICSD 615207), Pd_2N (ICSD 96418), Pd_2As (ICSD 26279), Pt_2Si (ICSD 77973), Ni_2S (hexagonal, ICSD 105342) and Ni_2S (orthorhombic, ICSD 165257). Matches were evaluated on the basis of MAD (Mean Angular Deviation), which is a measure of the misfit (in degrees) between observed and simulated Kikuchi bands. In general, MAD values < 1 indicate reasonable matches between the Kikuchi patterns obtained for an unknown and that calculated for a material. Through the evaluation undertaken in this study, only the match with the Kikuchi pattern calculated for Pd_2Si was found to give a MAD value < 1, in this case 0.34. The MAD values for all other matches were found to be large (all being > 1, most >2) and the phases from which they were calculated were disregarded. Given its stoichiometry and low MAD value, palladosilicide is thus considered to be isostructural with synthetic, metal-rich Pd_2Si and structurally, could be considered as the Pd-Si analogue of barringerite $(Fe,Ni)_2P$ (Buseck 1969).

The crystal structure of synthetic, metal-rich Pd_2Si (Fe_2P-type) has been solved and refined to *R* 9.2% (Nylund 1966). It has Pd in the 3*f* and 3*g* positions, with Si in the 2*c* and 1*b* sites.

Calculated cell data based on synthetic, metal-rich Pd_2Si (Nylund 1966) are as follows: Hexagonal, space group *P*-62*m*, *a* = 6.496(5), *c* = 3.433(4) Å, V = 125.5(1) $Å^3$, *c*:*a* = 0.529. Calculated and measured powder X-ray data for metal-rich Pd_2Si are listed in Table 6. The density could not be measured due to the small size of the grain being studied. Density (calc.) = 9.718 g cm^{-3} [sample D395/6(1)], 9.753 g cm^{-3} [D395/6(2), and 9.562 g cm^{-3} (sample Ct-2) using the derived empirical formulae; for sample numbers refer to Table 5.

Synthesis

The earliest account of the synthesis of Pd_2Si is by Buddery and Welsh (1951) and determined to be isotypic with Fe_2P (*C*22 type) by Anderko and Schubert (1953). These findings were confirmed by Grigorev et al. (1952). The Pd_2Si phase is reported to melt congruently at 1,330 ºC, based on thermal analyses (Hansen and Anderko, 1958). The crystal structure of metal-rich Pd_2Si (revised *C*22 type) was reported refined to be hexagonal, space group *P*62*m*, *a* = 6.496, *c* = 3.433 Å and Si-rich Pd_2Si to have a superstructure [*a* = 15.05(5) *c* = 27.49(0) Å] by Nylund (1966). However, it should be noted that Nylund's study was done before electron microprobes became readily available. Therefore phase equilibrium investigations usually required detailed metallographic studies together with X-ray diffraction analyses in order to determine phase boundaries, tie lines, and related information (e.g., Cabri 1965). It is noteworthy that Nylund reported it was extremely difficult to achieve thermodynamic equilibrium, but this aspect was not discussed further.

Classification, other occurrences of metal silicides

In the Nickel-Strunz classification, the mineral belongs to Elements, metallic carbides, silicides, nitrides and phosphides, 01.BB Silicides, 01.BB.36 palladosilicide Pd2Si, *P*-62m. In the Dana classification palladosilicide belongs to Suessite Group silicides, 01.01.23.08, palladosilicide Pd_2Si, *P*-62m; suessite $(Fe,Ni)_3Si$, gupeiite Fe_3Si, linzhiite $FeSi_2$, naquite FeSi, xifengite Fe_5Si_3, hapkeite Fe_2Si, luobusaite $Fe_{0.83}Si_2$, mavlyanovite Mn_5Si_3, and brownleeite MnSi.

Natural examples of metal silicides are rare, the first (suessite) having been reported from extraterrestrial objects (an olivine pigeonite achondrite, ureilite). Gupeiite and xifengite were found as cores of spheres 0.1-0.5 mm in diameter in placers in the Yanshan area, People's Republic of China (Yu 1984). They were found as heterogeneous grains,

with outer shells consisting of magnetite, wüstite, and maghemite, an inner shell of kamacite and taenite, and the cores being of either gupeiite or xifengite. The minerals present and the morphology of the spheres were thought to maybe extraterrestrial in origin.

Rudashevskii et al. (2001) gives the first account of several PGE-bearing, Fe- and Cu-silicides that were found in ferromanganese crusts that formed on the ocean floor in areas that were almost completely sediment-free. They ascribed formation of the base- and precious metal silicides to be related to emanations of highly reducing fluids that accompanied basalt formation.

Iron silicides have also been characterized as new minerals from podiform ophiolitic chromitites at Luobusha, Tibet (Bai et al. 2006, Li et al. 2012 a,b). Two of these minerals had previously been first reported by Gevork'yan (1969) and Gevork'yan et al. (1969) in heavy-mineral concentrates from placers and drill-core samples in sandstones from the Ukraine and described two new alloy minerals (FeSi and $FeSi_2$) but without approval by the CNMMN. Owing to their chemical properties and mineral assemblage, the Luobusha Fe silicides were considered to be xenocrysts from the mantle, transported to shallow depths by a rising plume and then captured by the melts from which the Luobusha chromitites crystallized (Bai et al. 2000, Yang et al. 2014).

Silicides may also form due to very high temperatures (e.g. 1,800ºC) such as "fulgurites", formed as a result of lightning strikes (e.g., Myers and Peck, 1925).

Genetic implications and discussion

In the case of palladosilicide, which appears to be the first report of a Platinum-Group Mineral (PGM) silicide, we have a few clues regarding its origin based on mineral associations. A few of the palladosilicide grains had some chromite attached and two were included

within chromite, strongly suggestive that the mineral crystallised in association with or within chromite. We have not studied the chemistry and zoning of the chromitite in our samples. The effect of highly reducing fluids during formation of mantle-derived ultramafic rocks was discussed by Rudashevskiy (1983), Rudashevskii (1984), and Rudashevskiy and Yertseva (1987). The formation and evolution of different chromitite deposits was recently reviewed and discussed by Mungall (2014) and Spandler et al. (2007) question the popular interpretation that anomalous melt inclusions represent samples of unmodified mantle melts. In light of the ease with which some chemical components can diffuse through chromite at magmatic temperatures, we infer that chromite may serve as a semi-permeable membrane allowing some constituents of the melt inclusions, but not others, to reach equilibrium with ambient conditions (James Mungall, personal communication 2014). Since chromite itself contains both ferric and ferrous iron, diffusive exchanges involving both of these species driven by counterfluxes of other cations might lead to extreme perturbations in f_{O2} within melt inclusions. Similarly extremely reducing mineral assemblages including moissanite (SiC), Fe-Si, and Fe-C phases have been reported from other chromitites (e.g., Bai et al. 2006; Yang et al., 2014).

We anticipate that this first report of a palladium silicide found in chromitite-rich facies of layered PGE-bearing intrusions will lead to further studies focused on understanding the chemical-physical and thermodynamic conditions directed to constraining the specific conditions under which such minerals crystalize. The presence of inclusions of a Ag telluride in one case and of a Pd-(Cu)-Sn mineral plus much smaller unidentified minerals in a second grain also call for a better understanding of phase equilibria in the Pd-Si-Ag-Te and the Pd-Si-Sn systems, as well as re-investigation of the Pd-Si binary.

Acknowledgements

We are grateful to management of the Goldstream Mining NL – Lonmin plc joint venture who gave permission to publish the results in 2005, when we first started this investigation. We also wish to acknowledge W.D. Maier for providing the location map used for Figure 1, Martine Wilhelmij for drafting Figure 2, Heinz-Juergen Bernhardt for help with German abbreviations, Jim Mungall for discussions pertaining to genetic aspects, and Peter Williams, Chairman of the CNMNC and its members for helpful comments on the submitted data.

References

Anderko, K. and Schubert, K. (1951) Kristallstructur von Pd_2Si, Pd_2Ge und Pt_2Ge. *Zeitschrift für Metallkunde*, **44**, 3017-312.

Bai, W, Robinson, P.T., Fang, Q., Yang, J., Yan, B, Zhang, Z., Hu, X., Zhou, M. and Malpas, J. (2000) The PGE and base-metal alloys in the podiform chromitites of the Luobusha ophiolite, southern Tibet. Canadian Mineralogist, **38**, 585-598.

Bai, W., Shi, N., Fang, Q., Li, G., Xiong, M., Yang, J. and Rong, H. (2006) Luobusaite: A New Mineral. Acta Geologica Sinica, **80**, no. 5, 656-659.

Buddery, J.H. and Welsh, A.J.E. (1951) Borides and silicides of the platinum metals. *Nature*, **167**, 362.

Buseck, P.R. (1969) Phosphide from “Metorites”: Barringerite, a New Iron-Nickel Mineral. Science, New Series, **165**, No. 3889, 169-171

Day, A. and Trimby, P. (2004) *Channel 5 Manual*. HKL Technology, Inc., Hobro, Denmark.

Cabri, L.J. (1965). Phase relations in the Au-Ag-Te system and their mineralogical significance. *Economic Geology*, **60**, 1569-1606.

Cabri, L.J. (2004) A mineralogical examination of samples from the Kapalagulu Intrusion, western Tanzania, for Goldstream Mining NL. **Confidential Report 2004-03**, 92pp.

346 Cabri, L.J., Rudashevsky, N.S. and Rudashevsky, V.N. (2008) Current
347 approaches for the process mineralogy of platinum-group element
348 ores and tailings. Ninth International Congress for Applied
349 Mineralogy ICAM 2008. *The Australasian Institute of Mining and*
350 *Metallurgy*, Publication Series No 8/2008, 9-17.

351 Cawthorn, R.G. (2002) Platinum-group element deposits in the Bushveld
352 Complex, South Africa. In: Cabri LJ (ed) The geology,
353 geochemistry, mineralogy and mineral beneficiation of platinum-
354 group element. *Canadian Institute Mining Metallurgy Petroleum*,
355 Spec. Vol. **54**, 389–430.

356 Gevork'yan, V.K. (1969) The occurrence of natural ferrosilicon in the
357 northern Azov region. Doklady Akademii Nauk SSSR, **185**, 416–
358 418 (in Russian).

359 Gevork'yan, V.K., Litvin, A.L., and Povarennykh, A.S. (1969) Occurrence
360 of the new minerals fersilicite and ferdisilicite. Geologichesky
361 Zapiski Akademii Nauk Ukrainskaya SSR, **29**, 2, 62–71 (in
362 Russian).

363 Grigorev, A.T., Strunina, T.A., and Adamova, A.S. (1952) *Investia Sektora*
364 *Platiny*, **27**, 219-222.

365 Hansen, M. and Anderko, K. (1958) Constitution of Binary Alloys.
366 Metallurgy and Metallurgical Engineering Series, *McGraw-Hill*
367 *Book Co.*, New York, pp. 1305.

368 Li, G., Bai, W., Shi, N., Fang, Q., Xiong, M., Yang, J., Ma, Z. and Rong,
369 H. (2012) Linzhiite, FeSi2, a redefined and revalidated new mineral
370 species from Luobusha, Tibet, China. European Journal of
371 Mineralogy, **24**, 1047–1052.

372 Li, G., Shi, N., Xiong, M., Ma, Z., Bai, W. and Fang, Q. (2012) Naquite,
373 FeSi, a new mineral species from Luobusha, Tibet, western China.
374 Acta Geologica Sinica, **86**(3), 553–538.

375 Maier, W.D., Barnes, S.-J., Bandyayera, D., Livesey, T., Li C., Ripley, E.
376 (2008). Early Kibaran rift-related mafic–ultramafic magmatism in
377 western Tanzania and Burundi: Petrogenesis and ore potential of
378 the Kapalagulu and Musongati layered intrusions. Science Direct
379 Lithos **101** (2008) 24-53.

Mungall, J.E. (2014) Geochemistry of Magmatic Ore Deposits, Reference Module in Earth Systems and Environmental Sciences, Treatise on Geochemistry 2nd Edition, **13**, Chapter 8, 195-218. http://dx.doi.org/10.1016/B978-0-08-095975-7.01108-6.

McDonald, A.M., Cabri, L.J., Stanley, C.J., Good, D.J., Redpath, J., Lane, G. and Spratt, J. (2014) Coldwellite, Pd_3Ag_2S, a new mineral from the Coldwell Complex, Ontario, Canada. *Canadian Mineralogist* (submitted).

Myers, W. M. and Peck, A.B. (1925) A fulgurite from South Amboy, New Jersey, *American Mineralogist*, **10**, 152-155.

Nylund, A. (1966) Some notes on the palladium-silicon system. *Acta Chemica Scandanavica*, **20**, 2381-2386.

Rudashevskii, N.S., Kretser, Y.L., Anikeeva, L.I., Andreev, S.I., Torokhov, M.P. and Kazakova, V.E. (2001) Platinum minerals in oceanic ferromanganese crusts. *Doklady Earth Sciences*, **378**, No. 4, 464-467.

Rudashevskiy, N.S. (1983) New features of differentiation of platinum group elements in the earth's crust. Doklady Akademii Nauk SSSR. **268**(1), 201-206. (English translation in Doklady Earth Science Sections, 1984, **268**, 178-182.)

Rudashevskii, N.S. (1984) A new model for the differentiation of elements of the platinum group in the lithosphere. Zapiski Vses. Mineral. Obsch. (1984) 113, #5, 521-539. (English translation, ref #1664907, Canmet Library, Ottawa. ON. Canada 1985, pp. 34.)

Rudashevskiy, N.S. and Yertseva, L. N. (1987) Diffusion of iron into platinum metals in platinoid mineralization in ultramafites. Geologiya rudnykh mestorozhdeniy, 1987. #6. 46-55. (English translation in International Geology Review, 1987 **29**, 1246-1253.)

Rudashevsky, N.S., McDonald, A.M., Cabri, L.J., Nielsen, T.D.F., Stanley, C.J., Kretser, Y.L., and Rudashevsky, V.N. (2004) Skaergaardite, PdCu, a new platinum-group intermetallic mineral from the Skaergaard intrusion, Greenland. *Mineralogical Magazine*, **68**, 603-620.

413 Schouwstra, R. P., Kinloch, E. D. and Lee, C.A. (2000) A short geological
414 review of the Bushveld complex. *Platinum Metals Review*, **44**, (1),
415 33-39.

416 Spandler, C., O'Neill, H. St C., and Kamenetsky, V. S. (2007) Survival
417 times of anomalous melt inclusions from element diffusion in
418 olivine and chromite. Nature, **447**, 303-306.

419 Wilhelmij, H.R. and Joseph, G. (2004) Stratigraphic location of platinum
420 mineralisation in the Kapalagulu intrusion of western Tanzania.
421 *Geoscience Africa* (Ed. L.D. Ashwal), vol. **2**, 709-708.

422 Wilhelmij, H.R. and Cabri, L.J. (in prep.) PGE-Ni-Cu mineralization in the
423 Kapalagulu Intrusion, western Tanzania.

424 Yang, J-S, Robinson, P. T. and Dilek, Y. (2014) Diamonds in ophiolite.
425 Elements, **10**, 127-130.

426 Yu, Z. (1984) Two new minerals gupeiite and xifengite in cosmic dusts
427 from Yanshan. Acta Petrologica Mineralogica et Analytica, **3**, 231-
428 238 (in Chinese with English abstract).

429

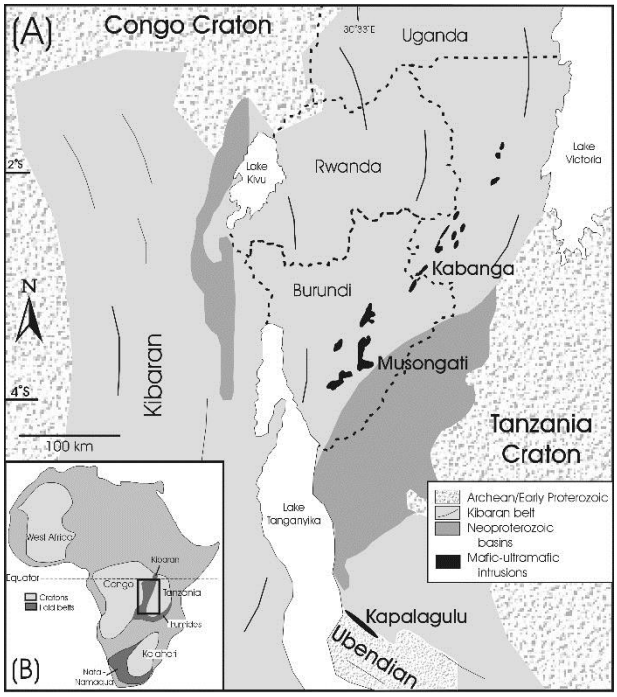

Figure 1. Location of the Kapalagulu Intrusion with respect to other intrusions of the Central African nickel belt (Maier et al. 2008).

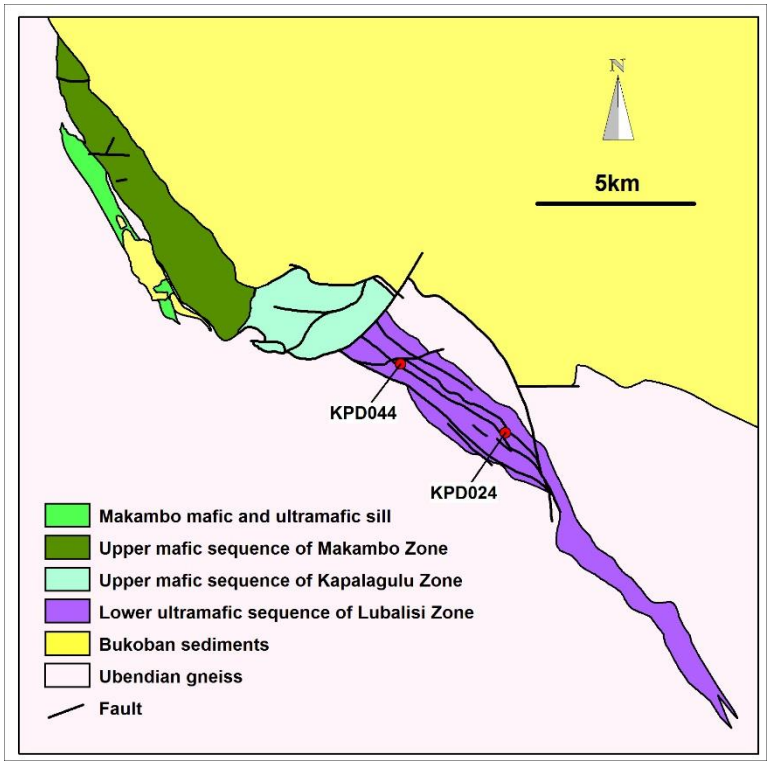

Figure 2. Geological map outlining the Kapalagulu Intrusion and the Lower Ultramafic Sequence present within a dyke-like body known as the Lubalisi Zone. Shown are the two drill holes from which the harzburgite samples containing the PGM were taken from.

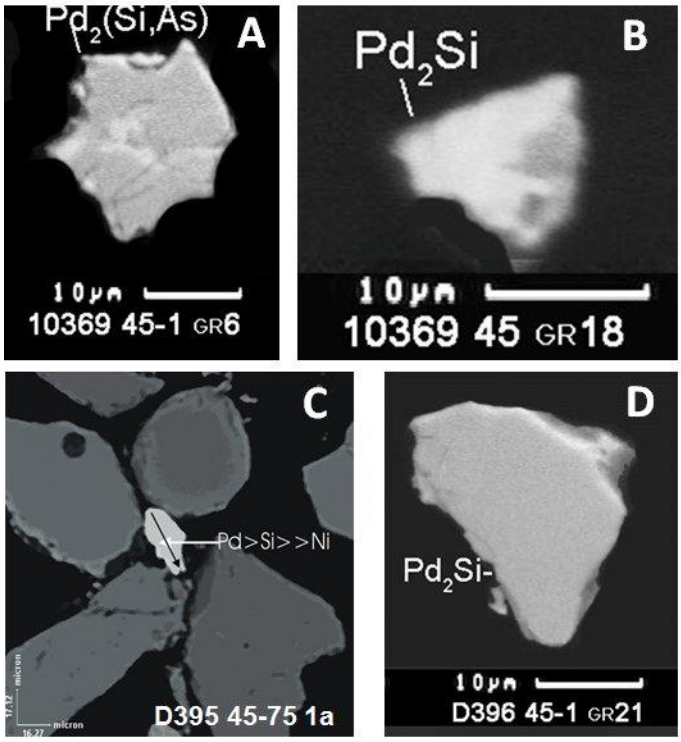

Figure 3. BSE images of four grains of the Pd silicide from the Kapalagulu intrusion.

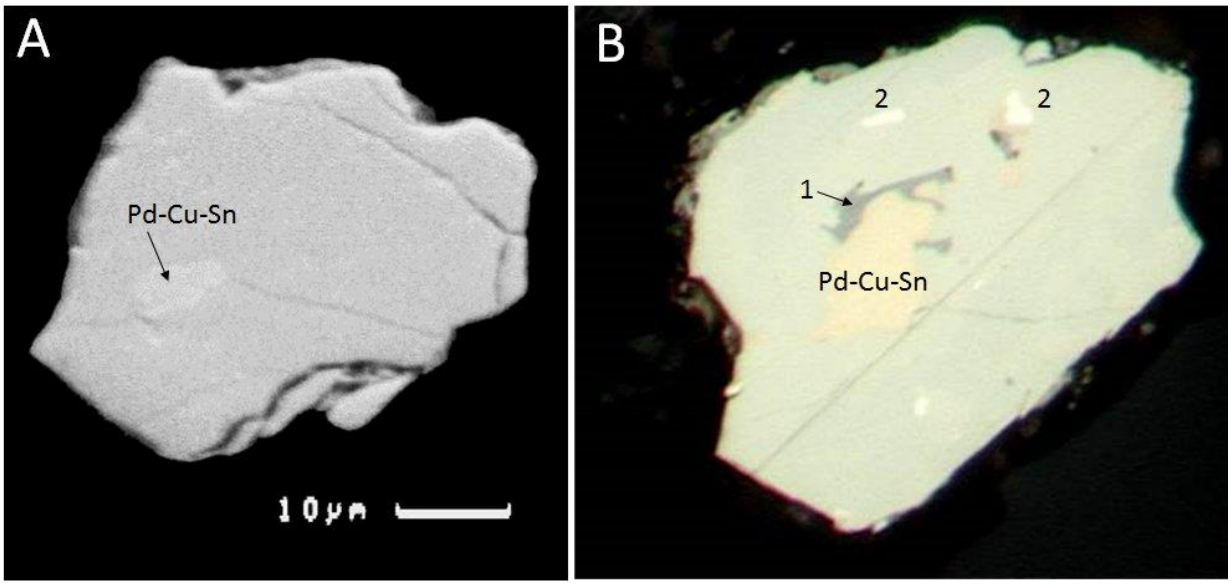

Figure 4. SEM image of Pd silicide (A) with inclusion of a Pd-(Cu)-Sn mineral and (B) showing more inclusions (1 and 2), as well as an enlarged area for the Pd-(Cu)-Sn mineral in reflected light. Sample from UG-2.

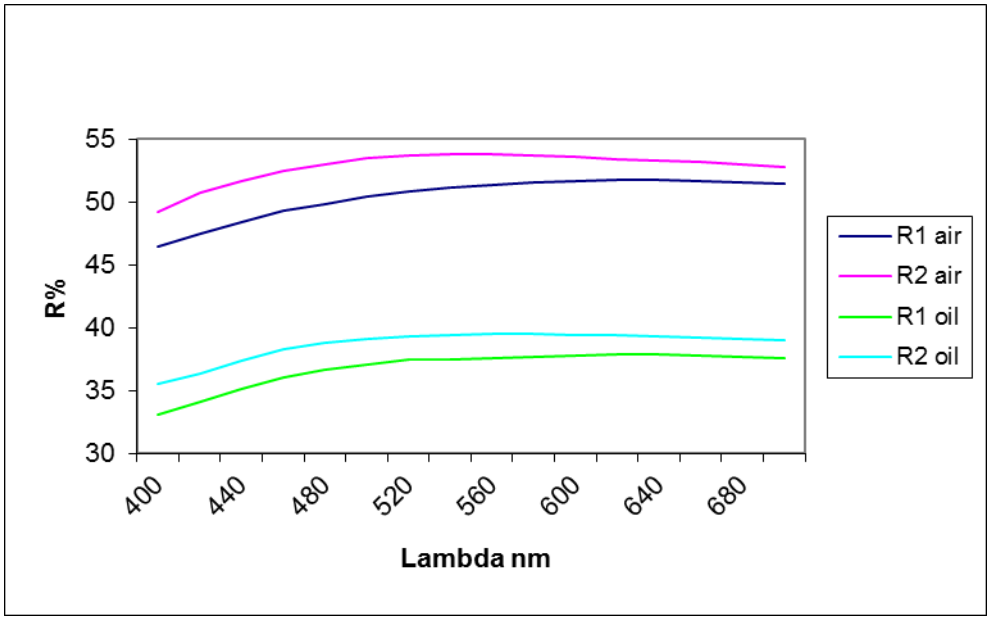

Figure 5. Reflectance data in air and oil for Pd_2Si, measured on grain from UG-2.

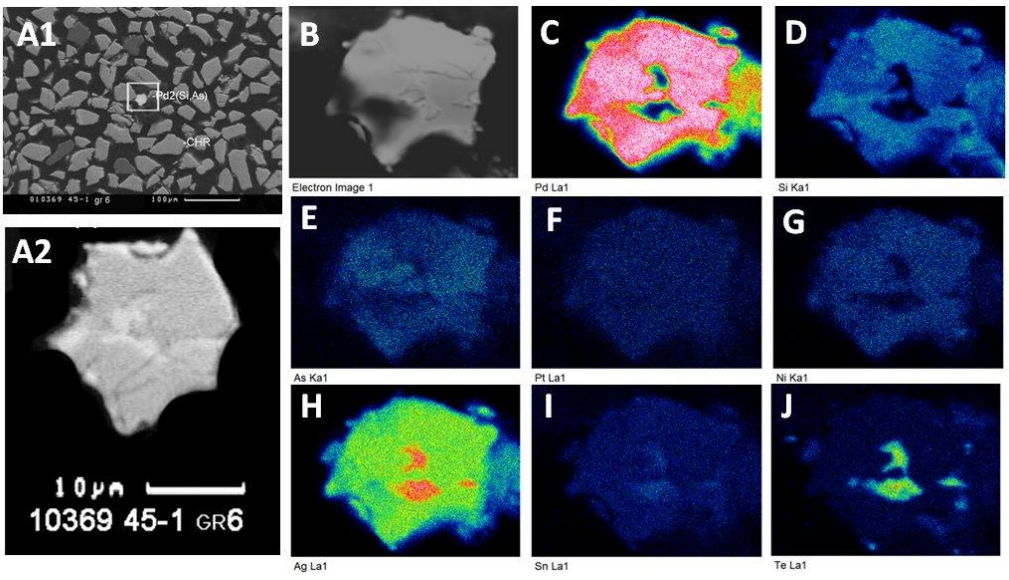

Figure 6. BSE images of grain 6 (sample 10369) and X-ray maps. A1 = BSE location map in hydroseparation concentrate; A2 = higher magnification BSE image of grain 6; the X-ray maps (B to J) are mirror images of A2. The Sn-bearing Ag-Te inclusion (bright areas in A2) shown in H, I, and J has an approximate composition of $Ag_{0.65}Te_{0.35}$, which corresponds to either hessite (Ag_2Te) or stützite ($Ag_{5-x}Te_3$).

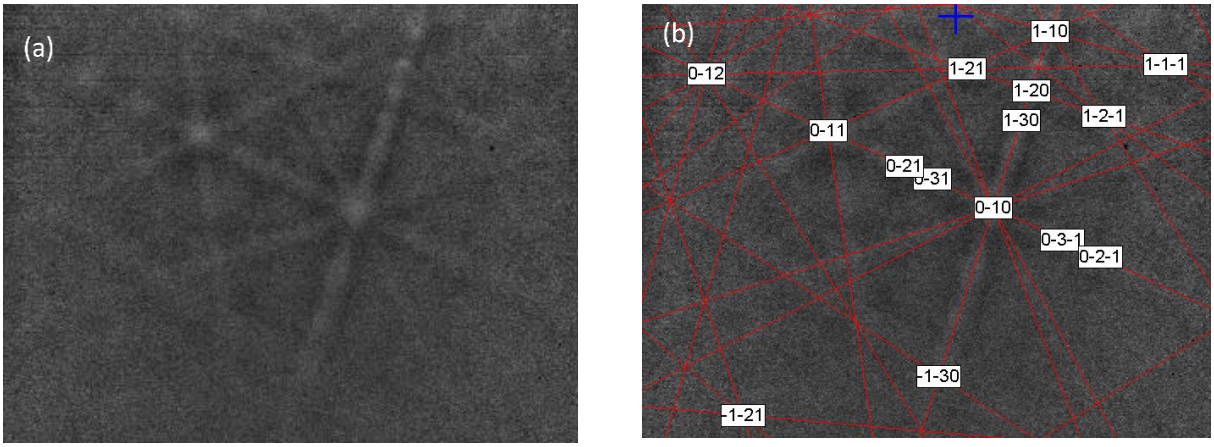

Figure 7. (a) The EBSD pattern for palladosilicide grain 6 (sample 10369); (b) the EBSD pattern for palladosilicide, indexed using data calculated from the crystal structure of synthetic Pd_2Si (Nylund. 1966).

526 Table 1. Precious metal minerals in heavy mineral concentrates from
527 Kapalagulu (sample 10369)

Mineral	**Frequency**	**Mass %**	**Volume%**
Ag>Au alloy	1	0.0	0.0
atokite	3	6.9	6.9
“electrum”	5	20.7	16.1
genkinite	1	0.1	0.1
Isoferroplatinum	1	0.4	0.2
keithconnite	3	0.0	0.1
kotulskite	3	4.2	4.6
mertieite-II	11	10.6	10.8
moncheite	42	14.4	16.1
palladium	2	0.7	0.5
palladosilicide	4	2.5	2.8
platinum	2	0.1	0.2
sobolevskite	2	5.5	5.3
sperrylite	21	31.8	33.8
stibiopalladinite	19	0.8	0.8
sudburyite	1	1.3	1.6
vysotskite	2	0.0	0.0
Total	123	100.0	100.0

528

529 Table 2. Colour values for palladosilicide (UG-2)

A illuminant				
x	0.451	0.448	0.451	0.449
y	0.41	0.41	0.41	0.41
Y%	51.3	53.6	37.6	39.4
λ d	583	576	582	579
P_e%	3.9	2.1	4.2	3
C illuminant				
x	0.315	0.312	0.315	0.313
y	0.322	0.321	0.323	0.322
Y%	51.2	53.6	37.5	39.4
λ d	573	567	572	569
P_e%	2.8	1.8	3.2	2.4

530

531 Table 3. Reflectance data measured on UG-2 grain in air and in oil[1]

	AIR		OIL	
λ	*R_1 (%)*	*R_2 (%)*	*R_1 (%)*	*R_2 (%)*
400	46.4	49.2	33.1	35.5
420	47.5	50.7	34.1	36.3
440	48.4	51.6	35.1	37.3
460	49.3	52.4	36.0	38.3
470	**49.6**	**52.7**	**36.3**	**38.6**
480	49.8	53.0	36.6	38.8
500	50.4	53.5	37.0	39.1
520	50.8	53.7	37.4	39.3
540	51.1	53.8	37.5	39.4
546	**51.2**	**53.8**	**37.6**	**39.5**
560	51.3	53.8	37.6	39.5
580	51.5	53.7	37.7	39.5
589	**51.6**	**53.7**	**37.8**	**39.5**
600	51.6	53.6	37.8	39.4
620	51.7	53.4	37.9	39.4
640	51.7	53.3	37.9	39.3
650	**51.7**	**53.3**	**37.9**	**39.3**
660	51.6	53.2	37.8	39.2
680	51.5	53.0	37.7	39.1
700	51.4	52.8	37.6	39.0

532

533

534

535

536

537

[1] Using a Zeiss WTiC standard in air and oil with n = 1.515.

538 Table 4. Electron probe microanalyses.

			Kapalagulu (sample D395 45-75 1a)				UG-2 (Ct-2)		
	LOD (ppm)	Ideal wt.%	wt.% [2]	wt.%[3]	Range (n=8)	St. dev.	wt.%	Range (n=12)	St. dev.
Si	204	11.66	8.51	7.95	6.83-8.58	0.68	10.13	8.49-10.76	0.88
Pd	244	88.34	70.03	68.56	64.20-70.69	2.01	68.77	66.35-72.27	2.14
Ag	1478		1.84	1.07	0.17-2.64	0.98	0.33	0.18-0.64	0.12
Ni	384		4.70	4.59	4.26-4.89	0.23	5.16	4.85-5.51	0.23
Te	456		0.47	0.32	0.00-1.16	0.43			
Sb	553		0.33	0.36	0.26-0.55	0.09	0.11	0.00-0.55	0.20
As	652		3.66	3.95	3.15-6.76	1.15	2.18	0.82-5.37	1.74
Fe	366		0.65	0.64	0.57-0.69	0.04	0.35	0.23-0.42	0.06
Pt	753		1.85	1.72	1.17-1.96	0.24	4.45	1.57-6.30	1.74
Sn	350		1.85	1.79	1.33-2.10	0.24	3.08	1.54-4.18	0.92
Cu	525		2.02	2.18	1.96-2.67	0.26	1.62	1.17-2.45	0.47
Rh	431		2.52	2.39	2.06-2.61	0.20	3.76	2.40-5.18	1.03
Totals		100	98.44	95.53	89.50-98.44		99.94	99.43-100.50	

539

540 Table 5. Atoms per formula unit for two grains analyzed by EPMA

	Kapalagulu (D395 45-75 1a)		UG-2 (Ct-2)
	Anal #1	n=8	n=12
Pd	1.636	1.657	1.557
Ni	0.199	0.201	0.212
Cu	0.079	0.088	0.061
Rh	0.061	0.060	0.088
Fe	0.029	0.029	0.015
Ag	0.042	0.026	0.007
Pt	0.024	0.023	0.055
Sn	0.039	0.039	0.063
Sum	**2.109**	**2.123**	**2.058**
Si	0.753	0.728	0.869
As	0.121	0.136	0.070
Sb	0.007	0.008	0.002
Te	0.009	0.006	
Sum	**0.890**	**0.878**	**0.941**
3 Atoms	**2.999**	**3.001**	**2.999**
D g cm^{-3}	**9.718**	**9.753**	**9.562**

541

[2] First analysis.
[3] Average of 8 analyses. After first analysis, epoxy softened, grain tilted and became covered with epoxy resulting in low totals

Table 6. Calculated and measured powder X-ray data for metal-rich Pd_2Si

Calculated*						Measured**	
λ = 1.54178Å; *a* = 6.496(5), *c* = 3.453(4) Å						λ = 1.54178 Å; *a* = 6.49, *c* = 3.43 Å***	
h	*k*	*l*	d_{calc}	I_{calc}****		d_{obs}	I_{obs}
0	1	0	5.6257	2			
1	1	0	3.2480	20		3.21	Weak
0	1	1	2.9429	8			
0	2	0	2.8129	1		2.83	Very weak
1	1	1	2.3658	100		**2.35**	**Very strong**
0	2	1	2.1808	34		**2.16**	**Strong**
1	2	0	2.1263	37		**2.12**	**Strong**
0	3	0	1.8752	19		**1.87**	**Medium**
1	2	1	1.8106	7		1.80	Weak
0	0	2	1.7265	12		**1.71**	**medium-**
2	2	0	1.6240	1			
1	3	0	1.5603	6		1.56	Weak
1	1	2	1.5245	3		1.51	Very weak
0	2	2	1.4714	0		1.47	Weak
2	2	1	1.4696	4			
1	3	1	1.4219	9		1.41	Medium
0	4	0	1.4064	1			
1	2	2	1.3403	11		**1.33**	**medium+**
0	4	1	1.3025	5		1.30	Weak
2	3	0	1.2906	2		1.29	Very weak
0	3	2	1.2702	7		1.26	medium-, broad
2	3	1	1.2089	10		**1.21**	**medium+,broad**
1	3	2	1.1576	3		1.15	Weak, broad
1	4	1	1.1567	1			
0	1	3	1.1276	0		1.12	Very weak
0	5	0	1.1251	1			
0	4	2	1.0904	1		1.09	Very very weak
1	1	3	1.0849	4		1.08	Weak
3	3	0	1.0827	1			
0	5	1	1.0698	2		1.07	Very weak
0	2	3	1.0653	2		1.06	Weak
2	4	0	1.0632	3			
2	3	2	1.0337	2		1.035	Weak
3	3	1	1.0331	0		1.029	Very very weak
2	4	1	1.0161	1			
1	2	3	1.0122	1		1.007	Weak
1	5	0	1.0104	2			
1	5	1	0.9697	2		0.968	Weak

*Using data of Nylund (1966) for synthetic metal-rich Pd_2Si. **Anderko and Schubert (1953) for synthetic Pd_2Si +~ 5% Pd_3Si, *i.e.*, metal-rich; abbreviations used by Anderko and Schubert (1953): sst = very strong, st = strong, m = medium, s = weak, ss = very weak, sss = very weak, and br = broad. ***Converted from kX units. ****Only for calculated I > or = 1.